The effects of reflected protons on the plasma environment of the moon for parallel interplanetary magnetic fields

J. S. Halekas,[1] A. R. Poppe,[1] J. P. McFadden,[1] and K.-H. Glassmeier[2]

Received 13 August 2013; revised 20 August 2013; accepted 21 August 2013.

[1] For the unique case of magnetic field parallel to the solar wind flow, a column of reflected protons can accumulate upstream from the Moon. We investigate observations from the ARTEMIS probes for an extended period with this geometry. During this time, P2 observes strong wave turbulence in two frequency bands above and below the ion cyclotron frequency near the Moon, not seen by P1 farther from the Moon. The lower frequency oscillations prove consistent with kinetic magnetosonic waves resonantly generated by reflected protons, and test particle calculations confirm that a significant column of reflected protons lies upstream when the waves occur. The reflected protons perturb a large volume of plasma around the Moon, extending upstream as well as into the wake. The waves observed near the Moon during this time period have many similarities to those found in the terrestrial foreshock and at comets, suggesting the potential for comparative studies.
Citation: Halekas, J. S., A. R. Poppe, J. P. McFadden, and K.-H. Glassmeier (2013), The effects of reflected protons on the plasma environment of the moon for parallel interplanetary magnetic fields, *Geophys. Res. Lett.*, *40*, doi:10.1002/grl.50892.

1. Introduction

[2] Until recently, the Moon was often considered a passive absorber of the solar wind. Observations from Nozomi first suggested that a significant fraction of incoming solar wind protons could reflect from localized regions of strong crustal magnetic fields [*Futaana et al*., 2003]. Recent data from Kaguya and Chandrayaan confirm that a significant percentage (up to 50%) of solar wind protons can reflect from crustal fields [*Lue et al*., 2011], and a small percentage (<1%) can reflect in charged form even from nonmagnetic regions [*Saito et al*., 2008]. Test particle calculations have addressed the trajectories of reflected protons [*Futaana et al*., 2003; *Holmström et al*., 2010], and indirect evidence exists that they drive significant low-frequency turbulence at low altitudes [*Tsugawa et al*., 2011; *Nakagawa et al*., 2012], but their effects on the plasma environment of the Moon remain largely unexplored.

[3] We now discuss the effects of reflected protons for the special case of interplanetary magnetic field (IMF) nearly parallel/antiparallel to the solar wind flow. In this geometry, reflected protons have small enough $\mathbf{E} \times \mathbf{B}$ drifts that they can travel farther than a single gyroradius upstream from the Moon (in principle, infinitely far, neglecting transfer of energy from particles to waves), thereby amplifying their effects on the incoming solar wind. Given the gyro-averaged drift velocity $\boldsymbol{v_D} = -(\boldsymbol{v}_{\mathrm{SW}} \times \boldsymbol{B}) \times \frac{\boldsymbol{B}}{B^2} = \boldsymbol{v}_{\mathrm{SW}} - (\boldsymbol{B} \cdot \boldsymbol{v}_{\mathrm{SW}}) \frac{\boldsymbol{B}}{B^2}$, the antiflow-aligned portion of the field-aligned component of the reflected proton velocity must satisfy $v_{R\|} cos\theta > |v_{\mathrm{SW}}| \sin^2\theta$ (with θ the angle between the IMF and the flow axis) for reflected protons to travel upstream. Assuming that protons can reflect with up to the full solar wind energy, with their velocity oriented at any angle relative to the solar wind, a finite percentage of reflected protons can therefore travel upstream for $\theta < 52°$. At nominal Parker spiral field angles, on the order of 45°, only ~29% of protons reflected from the subsolar point have velocities that satisfy the access condition derived above, and these still have primarily lateral velocities, such that they disperse rapidly from the vicinity of the Moon, and do not form a significant column for the incoming solar wind to encounter. However, at field angles on the order of ~10° or smaller, 90% or more of the reflected protons can travel upstream, with only a small lateral drift. For these conditions, the incoming solar wind can encounter a column of reflected protons that extends tens of thousands of kilometers upstream from the Moon, allowing wave growth to occur over several cyclotron periods, much longer than possible for oblique field angles.

2. Observations

[4] On 5 November 2012, the Moon, along with the two orbiting ARTEMIS probes, experienced an extended interval with the IMF nearly parallel to the solar wind flow velocity. Figure 1 shows an overview, utilizing data from the MAG [*Auster et al*., 2008] and ESA [*McFadden et al*., 2008] instruments. From ~3:35 until ~4:38, as it travels from a few thousand kilometers upstream and to the side of the Moon to the downstream wake flank, ARTEMIS P2 observes low-frequency waves (not seen by P1 in the undisturbed solar wind, upstream and 5000–10,000 km to the side of the Moon), with amplitudes of several nanotesla, in a frequency band of ~0.04–0.08 Hz (~0.5–1.0 Ω_i). A vestige of the low-frequency oscillations extends through the wake. Wavelet analysis shows that the low-frequency band contains primarily transverse wave power, with polarization varying from nearly circular to highly elliptical, and left-handed in the spacecraft frame. Near the wake boundary, compressional power increases significantly. For much of this period, we also observe an additional component at ~0.6 Hz. The higher-frequency waves have mainly transverse power and left-handed circular polarization in the spacecraft frame.

[1]Space Sciences Laboratory, University of California, Berkeley, California, USA.
[2]Institut für Geophysik und Extraterrestrische Physik, Technische Universität Braunschweig, Brunswick, Germany.

Corresponding author: J. Halekas, Space Sciences Laboratory, 7 Gauss Way, University of California, Berkeley, CA 94720, USA. (jazzman@ssl.berkeley.edu)

0094-8276/13/10.1002/grl.50892

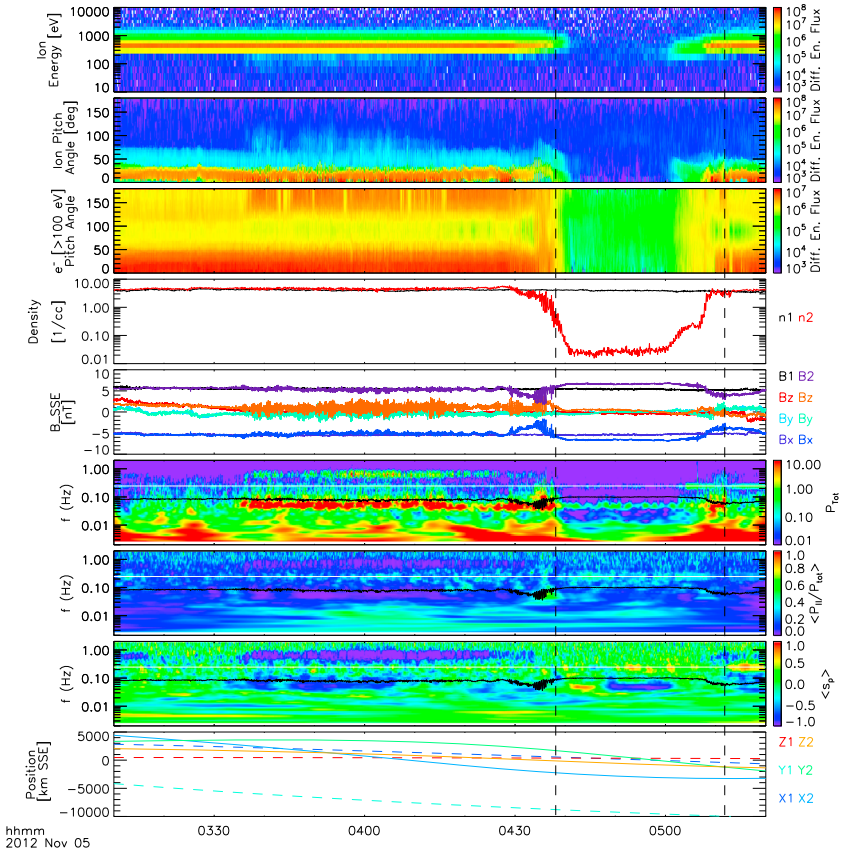

Figure 1. Ion differential energy flux (eV/(eV cm^2 s sr)) measured by P2 as a function of both energy and pitch angle, electron differential energy flux from P2 as a function of pitch angle, ion density from P2 near the Moon compared to that seen by P1 upstream, magnetic field components (Selenocentric Solar Ecliptic (SSE) coordinates) and magnitudes from P2 and P1, and total power, compressional fraction, polarization (positive = right handed) observed by P2 as a function of frequency, from wavelet calculations, and position (SSE) of both probes (P2 solid, P1 dashed). Black line on wavelet panels indicates local proton cyclotron frequency; white line indicates P2 spin frequency. Dashed lines indicate the extent of the optical shadow of the Moon.

We ignore spin tones, which have no clear orientation or polarization, consistent with measurement artifacts.

[5] At the same time, as the observed waves, P2 ESA data indicate the presence of significant perturbations to the local plasma, in the form of an ion population with energies below that of the bulk solar wind and primarily perpendicular velocities, and a counterstreaming electron population traveling upstream along the magnetic field opposite to the strahl. P1 (not shown) observes neither of these populations. These additional particle populations most likely represent the results of and/or drivers of the observed waves.

3. Wave Characteristics and Generation Mechanisms

[6] We now consider the low-frequency waves in more detail. Utilizing minimum variance analysis on the magnetic field (band-pass filtered to 0.02–0.1 Hz to focus on the low-frequency waves), we rotate the field into principal components. We show the unfiltered field, boxcar-smoothed with a window of ~1 Hz, in the minimum variance coordinates in Figure 2. At the first three times, the waves have well constrained principal axes, as indicated by the large ratio of intermediate and minimum eigenvalues. The waves have left-handed polarization in the spacecraft frame throughout the interval, with nearly circular polarization changing to more elliptical polarization, and the semimajor axis aligned roughly perpendicular to the wake boundary normal. As the probe approaches the wake, the waveforms become increasingly distorted, and the compressional component increases. Meanwhile, the inferred propagation direction rotates from almost perfectly parallel/antiparallel to the magnetic field to more oblique (the low eigenvector ratio indicates a poorly constrained propagation vector for the fourth interval). For the first three intervals, we can also see the smoothed signatures of the higher-frequency left-handed circular component, consistent with the wavelet analysis of Figure 1.

[7] For the low-frequency waves, the apparent left-handed polarization and frequency below the ion gyrofrequency suggest an anomalous resonant interaction with reflected protons, as proposed by *Nakagawa et al.* [2012] to explain similar waves at lower altitudes. If correct, this would imply right-handed waves generated and propagating upstream, but convected past the spacecraft by the solar wind flow and Doppler-shifted to an apparent left-handed polarization. Parallel-propagating waves would satisfy $\omega_{\rm obs} = \omega - kv_{\rm SW}$, and $\omega - k\left(v_{\rm SW} + v_{R||_x}\right) = -n\Omega_i$ (all variables positive). For the primary resonance $n = 1$, and $\omega_{\rm obs} = -X\Omega_i$ (X = 0.5–1.0 for this observation), we find $kv_{R||_x} = (1 - {\rm X}) * \Omega_i$ and $\omega/k = v_{\rm SW} - X/(1 - X) * v_{R||_x}$. For parallel-propagating magnetosonic

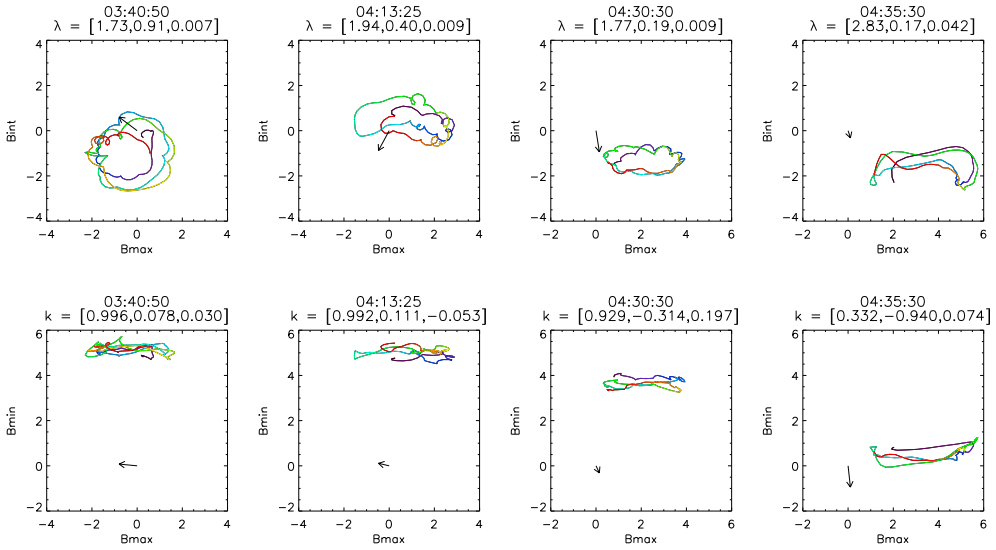

Figure 2. Magnetic field hodograms for four times during the time period of Figure 1, in minimum variance coordinates, with color representing time (purple/blue = start of sample and orange/red = end of sample) Top row labels indicate minimum variance eigenvectors, and bottom row labels indicate derived wave vector (parallel/antiparallel to the minimum variance direction), assuming upstream propagation. Arrows on each plot show projections of a unit vector from the origin pointing in the $-Y$ (SSE) direction, toward the Moon and its wake.

waves, we expect phase velocities on the order of the Alfvén speed ($v_A \sim v_{SW}/6$ for this time period), implying parallel proton velocities of $(1 - X)/X * 5/6 * v_{SW}$. For reflected protons with the full solar wind energy, this implies pitch angles of 147–90°, but if some reflect with less than the solar wind energy, the pitch angles of the resonant population could extend up to 180°. Therefore, resonant interactions with reflected protons can generate kinetic fast magnetosonic waves [*Krauss-Varban et al.*, 1994] consistent with our observations. In the solar wind frame, these right-handed waves would have frequencies of 0.1–0.2 Ω_i, and wavelengths of 6250–3125 km, strikingly similar to the "30 s" waves often observed in the terrestrial foreshock, and generally attributed to a similar mechanism [*Eastwood et al.*, 2005] (protons reflected from the Earth's bow shock rather than from lunar crustal magnetic sources).

[8] In order to better validate the scenario presented above, we conducted a test particle simulation to predict the distribution of reflected protons around the Moon. At each time step, we utilized the instantaneous magnetic field and flow velocity measured by the upstream probe P1 and analytically traced reflected proton trajectories. We launched protons uniformly over all accessible solid angles from every point on the upstream side of the Moon, with the same energy as the incident solar wind, and a weight corresponding to the reflection percentage measured by Kaguya and Chandrayaan [*Saito et al.*, 2008; *Lue et al.*, 2011]. We tracked each particle for eight gyroperiods, and accumulated all those that traveled within a lateral distance of 200 km from any point on a line parallel to the flow and intersecting the instantaneous P2 position. Figure 3 shows the resulting weighted relative density (arbitrarily normalized), as a function of time and distance along the flow axis from P2. Times with significant predicted accumulations of protons upstream from P2 (where not blocked by the solid lunar obstacle) correspond with the occurrence of waves, with the exception of a few minutes near the event onset at 3:35, and a brief period from 4:05–4:10 where the drift vector changed such that predicted trajectories just missed the region directly upstream from the probe. Given the large inferred parallel wavelengths, wave fronts could extend over a lateral range greater than a few hundred kilometers, at least up to the proton gyroradius of ~500 km. Also, given the large predicted upstream extent of the reflected proton column, even a very small amount of lateral propagation as the waves convect downstream could explain a slightly greater lateral extent at the spacecraft location.

[9] As an exercise, we conduct the same simulation, but with a nominal Parker spiral IMF imposed, and show the results in the bottom panel of Figure 3. In this case, most reflected protons cannot travel upstream, and those that do have large lateral velocities such that they do not accumulate upstream from the Moon, except within ~1–2 proton gyroradii from the surface. We would therefore expect disturbances to fill a much smaller volume for this configuration.

[10] The higher-frequency waves prove more difficult to uniquely explain. Given their observed frequency above the ion cyclotron frequency, only protons traveling downstream at a significant fraction of the solar wind speed would satisfy resonance conditions for intrinsically right-handed waves propagating upstream. Our test particle calculation suggests that few such particles should exist, and the non-solar wind ion population we observe locally has mostly perpendicular velocities, consistent with this expectation. Instead, these higher-frequency waves could represent whistlers excited by anisotropic and/or gyrating distributions, consistent with those expected for the reflected protons, as proposed by *Wong and Goldstein* [1987] to explain the strikingly similar "1 Hz whistlers" often observed in the foreshock. These waves may also prove responsible for scattering suprathermal electrons to form the counterstreaming distribution observed; alternatively, the counterstreaming electrons

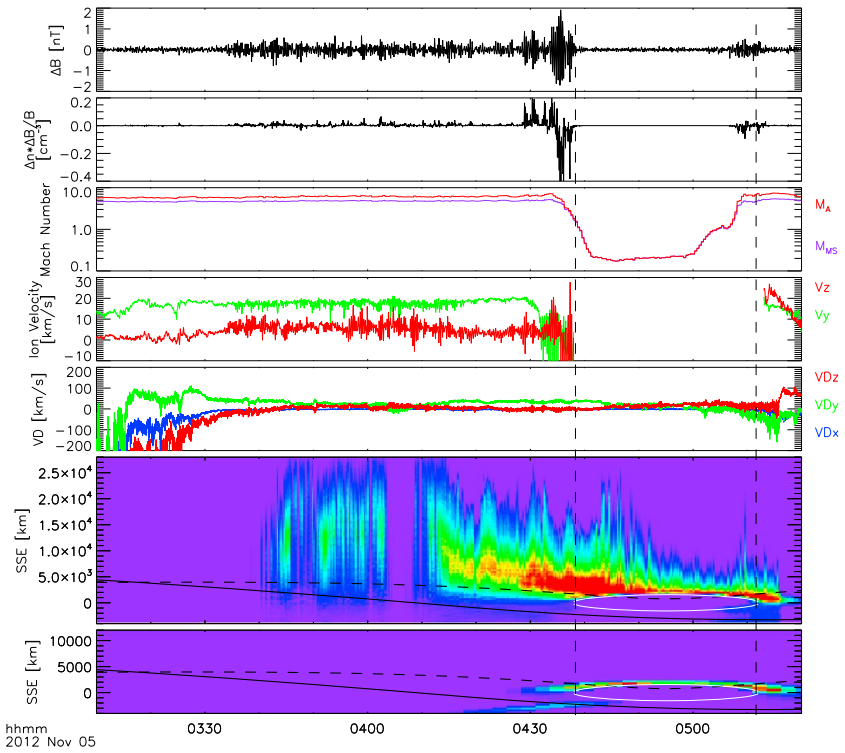

Figure 3. Compressional fluctuations in magnetic field magnitude, correlation between density and magnetic field fluctuations, ion Mach number, transverse ion velocity (not shown in wake), gyro-averaged $\mathbf{E} \times \mathbf{B}$ drift velocity from P1, and relative density of reflected ions upstream and downstream from ARTEMIS P2 predicted from test particle calculations (as a function of SSE X coordinate), for the actual IMF conditions, and for a nominal Parker spiral geometry, for the time period of Figure 1. Black lines in bottom two panels show P2 orbit in SSE coordinates (solid = X, dashed = $\sqrt{[Y^2 + Z^2]}$), and white ellipses outline the projection of the Moon in the plane of the orbit. Dashed vertical lines indicate the extent of the optical shadow of the Moon, as in Figure 1.

could result from the low-frequency waves and themselves produce the higher-frequency waves.

4. Interaction of Low-Frequency Waves With the Wake Boundary

[11] As described above, the low-frequency waves become more elliptical, more compressional, and more distorted as the P2 probe approaches the lunar wake boundary. These effects could in part result from larger densities of reflected protons near the limb, but test particle calculations predict that the reflected protons extend less far upstream from the probe near the limb, so the total upstream column most likely does not increase. Alternatively, the change in wave properties and distortion of the waveforms may result from interactions with the steep density gradient and the corresponding change in phase speed at the wake boundary. For wavelengths small compared to the width of the gradient, one could predict that magnetosonic waves should refract away from the wake; however, given the large wavelength and propagation nearly parallel to the boundary, this approximation most likely does not apply.

[12] Intriguingly, the apparent compressional component of the waves changes character with time, as demonstrated in Figure 3. Outside the wake, small compressive density and field fluctuations appear correlated, consistent with fast magnetosonic waves (in the kinetic regime, given the observed elliptical polarization). When the probe enters the rarefaction region, where the background magnetic field and density simultaneously decrease (see Figure 1), the compressional component of the observed waves increases dramatically, while still maintaining the same phase between density and field fluctuations. As the probe travels into the wake proper, where the background magnetic field increases (due to diamagnetic effects) and the plasma density decreases to near vacuum, the correlation of the observed density and magnetic field fluctuations reverses sign. When the probe reaches the submagnetosonic region in the central wake, compressional fluctuations essentially disappear.

[13] Given the correlation between changes in apparent wave properties and transitions between different regions of the wake, we suggest an interpretation of the observed signatures near the boundary not as purely propagating magnetosonic waves, but as driven motions of the wake boundary. In the rarefaction region, lateral movements of the boundary region across the slowly transiting probe will result in correlated fluctuations, while deeper in the wake, they will result in anticorrelated fluctuations, given the intrinsic properties of the wake. Therefore, velocity fluctuations associated with the parallel-propagating waves (with periods longer than the convection time from the limb to P2, and wavelengths longer than the down-wake distance) could drive boundary motions that would appear as compressional oscillations in the spacecraft frame. Before entering the wake, we observe transverse velocity fluctuations associated with the low-frequency waves, with a ~10–20 km/s peak-to-peak amplitude. Larger fluctuations exist near the wake, but here we cannot easily separate perturbations

associated with wake refilling from those due to the waves. Even a 10–20 km/s perturbation in transverse velocity would shift the local wake boundary by a lateral distance of ~60–120 km at P2's location, possibly sufficient to explain the observed fluctuations, given the steep plasma gradient near the boundary. Though δVy should have proportionally larger effects given the P2 location close to the ecliptic, δVz has greater magnitude and may also play a role. If correct, the observed features would represent a superposition of the convecting parallel-propagating waves and driven motions of the boundary as it flaps back and forth in response to velocity fluctuations associated with the waves.

5. Implications

[14] The low-frequency waves observed around the Moon have very similar characteristics to those observed in the ion foreshock and may also have similar origins. Most likely, no shock exists at the Moon; therefore, the lunar environment may afford an opportunity to separate phenomena generated at the shock from those driven locally by reflected particles. For the case with IMF parallel to the flow, low-frequency wave turbulence driven by reflected protons will fill a region many thousands of kilometers around the Moon, including a portion of the upstream region. For more oblique fields, similar effects should prove weaker and/or less extended, but do still exist to some degree, as confirmed by low-altitude observations [*Nakagawa et al*., 2012; *Tsugawa et al*., 2011]. This adds a new element to the conclusions of *Halekas et al*. [2012], which showed that electron-driven precursor effects also extend well upstream from the Moon, in both the solar wind and terrestrial magnetosphere.

[15] Another intriguing phenomenon may occur for the parallel IMF case. In this unique geometry, ionized exospheric constituents will not feel a strong convection electric field, allowing the buildup of larger heavy ion densities than normally possible in the region directly upstream from the Moon. These heavy ions could also drive waves, much as at comets. At low altitudes above the upstream side, for IMF parallel to the flow, such waves might prove observable (given the probe location downstream and to the side of the Moon for this time period, we would not necessarily observe these waves, depending on their properties), perhaps enabling a new technique to constrain the poorly known composition of the lunar exosphere.

[16] **Acknowledgments.** We acknowledge NASA grant NNX13AJ97G for supporting this study and ISSI for hosting a workshop that in part inspired this work. K.H.G. was financially supported through the German Ministry for Economy and Technology and the German Center for Aviation and Space (DLR) under contract 50 OC 1001.

[17] The Editor thanks Tomoko Nakagawa and an anonymous reviewer for their assistance in evaluating this paper.

References

Auster, H. U., et al. (2008), The THEMIS fluxgate magnetometer, *Space Sci. Rev.*, *141*, 235–264.

Eastwood, J. P., E. A. Lucek, C. Mazelle, K. Meziane, Y. Narita, J. Pickett, and R. A. Treumann (2005), The foreshock, *Space Sci. Rev.*, *118*, 41–94.

Futaana, Y., S. Machida, Y. Saito, A. Matsuoka, and H. Hayawaka (2003), Moon-related nonthermal ions observed by Nozomi: Species, sources, and generation mechanisms, *J. Geophys. Res.*, *108*(A1), 1025, doi:10.1029/2002JA009366.

Halekas, J. S., et al. (2012), Lunar precursor effects in the solar wind and terrestrial magnetosphere, *J. Geophys. Res.*, *117*, A05101, doi:10.1029/2011JA017289.

Holmström, M., M. Weiser, S. Barabash, Y. Futaana, and A. Bhardwaj (2010), Dynamics of solar wind protons reflected by the Moon, *J. Geophys. Res.*, A06206, doi:10.1029/2009JA014843.

Krauss-Varban, D., N. Omidi, and K. B. Quest (1994), Mode properties of low-frequency waves: Kinetic theory versus Hall-MHD, *J. Geophys. Res.*, *99*, 5987–6009.

Lue, C., Y. Futaana, S. Barabash, M. Wieser, M. Holmström, A. Bhardwaj, M. B. Dhanya, and P. Wurz (2011), Strong influence of lunar crustal fields on the solar wind flow, *Geophys. Res. Lett.*, *38*, L03202, doi:10.1029/2010GL046215.

McFadden, J. P., C. W. Carlson, D. Larson, M. Ludlam, R. Abiad, B. Elliott, P. Turin, M. Marckwordt, and V. Angelopoulos (2008), The THEMIS ESA plasma instrument and in-flight calibration, *Space Sci. Rev.*, *141*, 277–302.

Nakagawa, T., A. Nakayama, F. Takahashi, H. Tsunakawa, H. Shibuya, and H. Shimizu (2012), Large-amplitude monochromatic ULF waves detected by Kaguya at the Moon, *J. Geophys. Res.*, A04101, doi:10.1029/2011JA017249.

Saito, Y., et al. (2008), Solar wind proton reflection at the lunar surface: Low energy ion measurements by MAP-PACE onboard SELENE (KAGUYA), *Geophys. Res. Lett.*, *35*, L24205, doi:10.1029/2008GL036077.

Tsugawa, Y., N. Herada, Y. Katoh, T. Ono, H. Tsunakawa, F. Takahashi, H. Shibuya, and M. Matsushima (2011), Statistical analysis of monochromatic whistler waves near the Moon detected by Kaguya, *Ann. Geophys.*, *29*, 889–893.

Wong, H. K., and M. L. Goldstein (1987), Proton beam generation of whistler waves in the Earth's foreshock, *J. Geophys. Res.*, *92*, 12,419–12,424.